ANL/NE-12/4

The SAS4A/SASSYS-1 Safety Analysis Code System

Nuclear Engineering Division

ANL/NE-12/4

The SAS4A/SASSYS-1 Safety Analysis Code System

Chapter 13:
Cladding Motion Model — CLAP

Nuclear Engineering Division
Argonne National Laboratory

January 31, 2012

TABLE OF CONTENTS

LIST OF FIGURES

LIST OF TABLES

NOMENCLATURE

Symbol	Definition	Units
A_c	Moving cladding cross-sectional area	m^2
AFRV	Input constant in single-phase friction factor formula, Eq. 13.2-5	
A_f	Total area allowed for cladding by the fuel	m^2
A_{max}	Available area for molten cladding	m^2
A_s	Refrozen steel cross-sectional area	m^2
A_v	Vapor flow area	m^2
a	Constant in viscosity Eq. 13.2-18a	K
BFRV	Input constant, see AFRV	--
b_f	Molten cladding/pin turbulent friction factor, Eq. 13.2-16b	--
C	Liquid-steel volumetric coefficient of thermal expansion, Eq. 13.2-39	K^{-1}
C_a	Mass convection term	kg/m-s
C_f	Terms in the outer-fuel-node energy Eq. 13.3-17	W/m
C_m	Momentum convection term	m/s^2
C_v	Energy convection term, Eq. 13.3-9	W/m
C_1, C_2, C_3	Input constants in the correlation of liquid metal heat transfer,	
c_f	Eq. 13.2-28	--
c_{pc}	Coefficient of friction with fuel pin, Eq. 13.2-15	--
c_{pf}	Molten cladding specific heat capacity	J/kg-K
c_{ps}	Fuel specific heat capacity	J/kg-K
D_c	Solid steel specific heat capacity	J/kg-K
D_c	Molten cladding hydraulic diameter	m
D_h	Hydraulic diameter for bare fuel or fuel pin	m
D_v	Hydraulic diameter for the vapor	m
e_c	Moving cladding internal energy	J/kg
e_c^o	Constant, Eq. 13.2-42	J/kg
e_s	Refrozen steel internal energy	J/kg
F_p	Pin/molten-cladding friction force per unit volume of molten cladding	N/m^3
F_v	Cladding/vapor interfacial force per unit volume of channel	N/m^3
f	Melt fraction	--

Symbol	Definition	Units
fps	Full-power seconds from initial cladding motion	s
$(fps)_0$	Constant in incoherence factor on friction, Eq. 13.2-11	s
f_{sf}	Single-phase friction factor for vapor	--
g	Gravitational constant	m/s^2
h	Coefficient of heat transfer to the molten cladding from the solid interface	W/m^2-K
I	Incoherence multiplier on friction	--
j	Index for axial segment	--
ΔK	Reactivity change due to cladding relocation	$\delta k/k$
k_c	Molten cladding thermal conductivity	W/m-K
k_f	Fuel thermal conductivity	W/m-K
M	Friction multiplier due to flooding (M is also the total steel mass in channel)	--
m_j	Mass of cladding in segment j	kg
m_j^o	Initial mass of cladding in segment j	kg
$\dot{m}_c$	Mass rate of cladding melting per unit length of channel	kg/m-s
$\dot{m}_v$	Rate of vapor generation per unit length of channel	kg/m-s
n	Index for time step	--
P_e	Outer perimeter of intact cladding	m
P_r	Perimeter of the cladding solid/liquid interface	m
P/D	Pitch-to-diameter ratio for fuel pins	--
$\partial p/\partial z$	Channel axial pressure gradient	Pa/m
Q_j	Cumulative pin segment heat loss from beginning of heat transfer time step	J
Q_{NT}	Volumetric heat generation in outer fuel segment	W/m^3
q	Input constant, Eq. 13.2-18b	--
Re	Molten cladding Reynolds number, Eq. 13.2-17	--
$(Re)_{break}$	Turbulent transition Reynolds number, Eq. 13.2-16	--
$(Re)_v$	Reynolds number for vapor	--
r	Radius (from fuel pin axis)	m
r_{NR},r_{NT}	Fuel radii defined in Fig. 13.3-1	m
Δr_c	Half-thickness of molten cladding layer	m
Δr_i	Half-thickness of the intact cladding	m
Δr_s	Half-thickness of the refrozen cladding	m

Symbol	Definition	Units
Δr_w	Half-thickness of the structure	m
T_c	Moving cladding temperature	K
T_f	Fuel surface temperature	K
T_i	Intact cladding temperature	K
T_m	Cladding melting temperature	K
T_{ref}	Reference temperature in density Eq. 13.2-38	K
T_s	Refrozen cladding temperature	K
T_w	Structure temperature	K
t	Time	s
t*	Time at beginning of current heat-transfer time step	s
Δt	CLAP (coolant) time step	s
Δt^*	Heat-transfer time step	s
v_c	Moving cladding velocity	m/s
v_{flood}	Flooding velocity	m/s
W_j	Cladding reactivity worth distribution	∂k/k-kg
w	Vapor mass flowrate	kg/s
w_j	Segment midpoint mass flow, Eq. 13.3-14	kg/s
w_j^*	Segment boundary mass flow, Eq. 13.3-10	kg/s
$w_{m,j}$	Segment mean mass flow, Eq. 13.3-11	kg/s
x	Constant in incoherence factor on friction, Eq. 13.2-11a	--
y_1, y_2	Constants in linearized pin friction equation	N/m^3
z	Elevation	m
z_j	Segment boundary elevation	m
$z_{m,j}$	Nodal elevation, Eq. 13.3-13	m
Δz_j	Segment length	m
α	Vapor fraction based on area available for molten steel and vapor	--
α_{crit}	Input constant in two-phase multiplier, Eq. 13.2-10	--
β	Steel (solid) coefficient of linear thermal expansion, Eq. 13.2-38	K^{-1}
Γ	Factor in correction of cladding area for overfilled segments	m^3
γ_c	Computer coefficient, Eq. 13.3-22	
γ_f	Computed coefficient, Eq. 13.3-19	
ε	Input constant in two-phase multiplier, Eq. 13.2-10	--

Symbol	Definition	Units
θ	Multiplier on heat loss to structure (usually = 1)	--
λ	Effective heat-of-fusion, Eq. 13.2-26	J/kg
λ^o	Thermodynamic heat-of-fusion	J/kg
μ_c	Moving cladding viscosity	Pa-s
μ_m	Cladding viscosity at the liquidus temperature	Pa-s
μ_s	Solid cladding pseudo-viscosity, Eq. 13.2-18c	Pa-s
μ_t	Cladding viscosity at the solidus temperature	Pa-s
μ_v	Vapor viscosity	Pa-s
ξ_f, ξ_w	Computed coefficients	--
ξ_1, ξ_2, ξ_3	Computed coefficients	--
ρ_c	Molten cladding density	kg/m^3
ρ_c°	Density of cladding at the liquidus temperature	kg/m^3
ρ_f	Fuel density	kg/m^3
ρ_s	Refrozen steel density	kg/m^3
ρ_s°	Solid cladding density at the reference temperature	kg/m^3
ρ_v	Vapor density	kg/m^3
ϕ	Sensible heat flux from refrozen cladding to the molten interface	W/m^2
ϕ_c	Flux of sensible heat into the moving cladding layer	W/m^2
ϕ_{hf}	Fusion heat flux, Eq. 13.2-24	W/m^2
ϕ_r	Heat flux at interface of intact and refrozen cladding	W/m^2
ϕ_{trial}	Trail heat flux, Eq. 13.2-36	W/m^2
ϕ_1	Heat flux, Eq. 13.2-34	W/m^2
ϕ_2	Heat flux, Eq. 13.2-35	W/m^2
$\bar{\psi}$	Mean ratio of thermal-to-momentum eddy diffusivities	--

CLADDING MOTION MODEL — CLAP

13.1 Introduction and Overview

13.1.1 Background and Description of the CLAP Physical Model

The CLAP Model [13-1, 13-2] computes cladding relocation and phase changes for accident situations in which the fuel geometry is still essentially intact. Such a situation typically arises in undercooling accidents during which coolant voiding and pin dryout occur, followed by rapid heating and subsequent melting of the cladding. In the usual accident scenario, the cladding motion proceeds as follows: (i) the molten cladding may initially rise due to the pressure gradient and viscous shear forces generated by the sodium coolant vapor flow in the dried-out section of the core, (ii) the rising molten cladding then freezes upon encountering cooler structure in the region immediately above the active fuel (either the upper reflector or upper blanket region, depending upon the reactor design), and (iii) the upper frozen-cladding blockage throttles the vapor flow, thus allowing the remaining molten cladding to drain under the influence of gravity. The cladding motion and phase changes significantly affect the subsequent course of events in the scenario both through the influences of cladding-motion-related reactivity changes and frozen-cladding blockages that possibly inhibit later fuel motions.

The available SAS3D cladding relocation model, CLAZAS [13-3], is inflexible in calculation of the consequences for such diverse mechanistic and/or postulated phenomena. This model suffers from several shortcomings in the estimation of cladding accelerations. First, the use of large cladding segments can lead to a significant change in results following relatively minor input changes. Second, the model-dependent Lagrangian mesh leads to difficulties in integrating consistently with the voiding dynamics and fuel motion models. Third, the formalism does not provide flexibility with respect to the mode of cladding refreezing or with respect to variations in the time-dependent coupling to the sodium-vapor dynamics. If treated correctly, the influence of sodium-vapor dynamics could result in a possible display of oscillatory effects.

The CLAP model uses and Eulerian numerical formulation coupling the time-dependent continuity, momentum, and energy equations for a film of moving cladding, the continuity and energy for sodium vapor, and the SAS4A pin heat-transfer calculation. This is accomplished by interconnecting an implicit solution for the low-density sodium vapor with an explicit, modified upwind differencing procedure for the high-density cladding. Axial resolution depends on the mesh spacing selected by the user. The key phenomena influencing cladding motion in CLAP are the degree of interfacial sodium vapor friction and the cladding heat transfer. Input that controls these phenomena permits a variety of experimental situations to be simulated.

As shown in the schematic in Fig. 13.1-1, the CLAP model divides the core axially into two types of zones. In the central zone, the cladding is molten and is in motion. In that region, heat is transferred directly from the fuel surface to the molten cladding. In the zones at either end of the fueled region is intact cladding. Due to cladding motion, the intact cladding may be coated with refrozen cladding and/or molten cladding.

13.1.2 CLAP Module Structure and Interaction with Other SAS4A Models

The initiation of CLAP and the decision for adding axial segments to the molten-cladding zone occurs in the fuel-pin model TSHTRV. During cladding motion, the fuel-pin model TSHTRV continues to evaluate the fuel temperatures and, outside of the molten zone, the temperatures of the intact cladding. Coupling between TSHTRV and CLAP allows for heat transfer between the fuel and molten cladding in the molten-cladding zone and between the initial cladding and refrozen (or molten) cladding outside the molten zone.

The CLAP subroutines are called every coolant time step and, as shown in Fig. 13.1-2, are called from various locations in the sodium voiding module. The functions of the CLAP subroutines are as follows:

TSCLD1 - (i) initiates CLAP variables, (ii) adds segments to molten zone, (iii) calculates local heat transfer between molten steel and fuel within the molten zone, (iv) calculates local heat transfer between the initial cladding, refrozen cladding (if any), and molten cladding (if any) outside of the molten zone, and (v) computes mass and areas of the refrozen and molten cladding allowing for convection and phase change;

TSCLD2 - solves the momentum equation to obtain the velocity of the molten cladding film and contains the CLAP output and debug print statements;

SODFRC - computes the two-phase friction factor used to evaluate the interfacial shear stress between the sodium vapor and molten steel;

DENSIT - evaluates the cladding melt fraction, temperature, and density as a function of cladding specific internal energy.

The CLAP subroutine TSCLD1 computes the current (local) vapor flow areas and hydraulic diameters, which are used by the sodium voiding model. Also, TSCLD1 may reduce the current coolant time step, if necessary (based on a Courant condition criterion), and require the coolant dynamics model to reevaluate current flow parameters.

The CLAP subroutine TSCLD2 is called later and utilizes updated sodium vapor velocities and pressures to compute the molten cladding velocity for the beginning of the next time step. Local two-phase friction factors (to evaluate the gas/liquid interfacial stress), which are computed by TSCLD2 for the next time step, are passed to the sodium voiding model.

Coupling of CLAP with the reactivity model consists of current cladding mass distributions (axial) computed in TSCLD1 being utilized in the subroutine FEEDBK to evaluate the reactivity change due to cladding relocation.

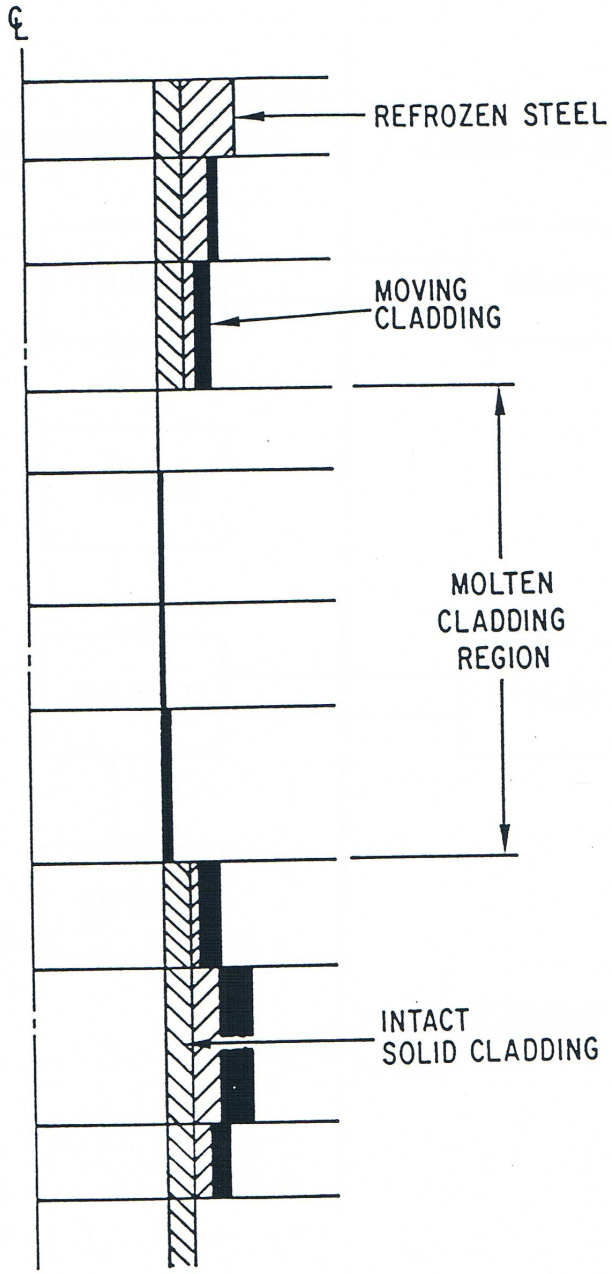

Fig. 13.1-1. Schematic of CLAP Geometry Treating Cladding Relocation

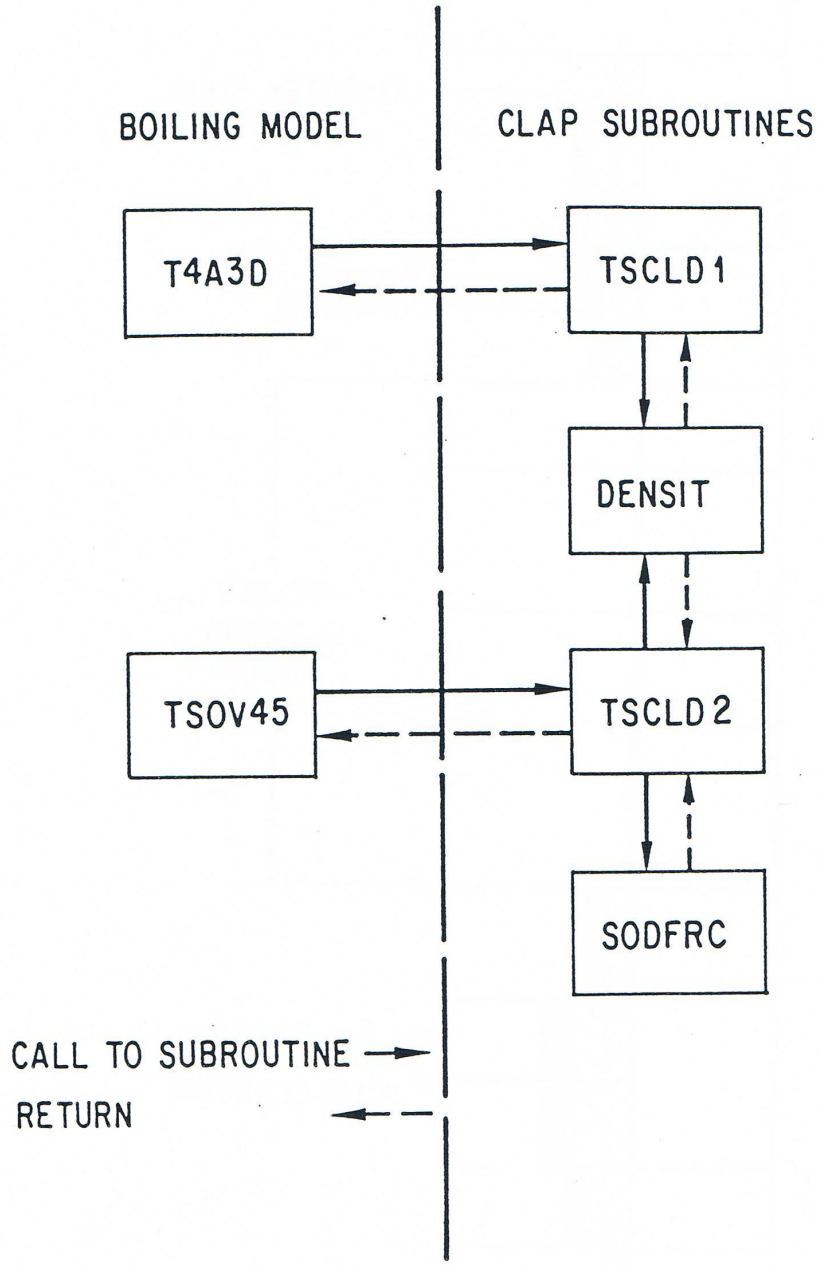

Fig. 13.1-2. CLAP Flowchart

13.2 Mathematical Model

13.2.1 Sodium Vapor Flow Model

The sodium vapor flow generates the axial pressure gradients and interfacial shear forces, which influence the motion of molten cladding. The cladding motion in turn changes flow areas, hydraulic diameters, and surface roughness which all affect the sodium vapor flow. The governing equations for the sodium vapor, while presented elsewhere (Section 12.6.1) in more detail, are reproduced here to show the intimate coupling between the sodium vapor dynamics and cladding motion. The conservation equations for the sodium vapor are

$$\frac{\partial}{\partial t}\left(A_v \rho_v\right) + \frac{\partial w}{\partial z} = \dot{m}_v \tag{13.2-1}$$

$$\frac{\partial w}{\partial t} + \frac{\partial}{\partial z}\left(w^2 / A_v \rho_v\right) + A_v\left[\frac{\partial p}{\partial z} + F_v\right] = \begin{cases} \dot{m}_v w / A_v \rho_v, & \text{if condensing} \quad (13.2\text{-}2a) \\ 0, & \text{if vaporizing} \quad (13.2\text{-}2b) \end{cases}$$

where

A_v = vapor flow area

ρ_v = vapor density

w = vapor mass flowrate

$\dot{m}_v$ = the rate of vapor generation per unit length of channel

$\frac{\partial p}{\partial z}$ = channel axial pressure gradient

F_v = cladding/vapor interfacial friction force per unit volume of vapor.

The friction force term is evaluated from the following equation:

$$F_v = \frac{f_{sf} M\, w\, |w|}{2\, \rho_v\, A_v^2\, D_v} \tag{13.2-3}$$

where

f_{sf} = single-phase friction factor

M = flooding multiplier

D_v = hydraulic diameter for the vapor.

The hydraulic diameter is estimated by

$$D_v = D_h \sqrt{\alpha} \tag{13.2-4}$$

where

D_h = hydraulic diameter for bare fuel or fuel pin (depending upon the zone)

α = vapor fraction based on area available for molten steel plus vapor.

This equation assumes that the hydraulic diameter D_v varies as the square root of the area $_v$ (which would be exact for a circular vapor flow passage) and hence scales as the square root of vapor fraction (proportional to the flow area).

The smooth wall (single-phase) friction factor is given by

$$f_{sf} = AFRV \left(\mathrm{Re}\right)_v^{BFRV} \tag{13.2-5}$$

$$\left(\mathrm{Re}\right)_v = wD_v / A_v \mu_v \tag{13.2-6}$$

where

AFRV, BFRV = input constants

μ_v = vapor viscosity.

For consistency, the inputed constants AFRV and BFRV used in CLAP are identical to those used in the sodium voiding model.

The flooding multiplier is flow-regime dependent. The transition from smooth wall friction (M = 1) to a chaotic two-phase flow structure ($M = M_{2\Phi}$, where $M_{2\Phi}$ is defined later) occurs nominally when the vapor velocity exceeds the flooding velocity. The current version of CLAP uses the correlation of Fauske, et al. [13-4]:

$$v_{flood} = \left[\frac{32}{3} \frac{\rho_c \, g \Delta r_c}{\rho_v \, f_{sf} \, M_{2\Phi}} \right]^{1/2} \tag{13.2-7}$$

where

Δr_c = one-half the molten cladding thickness

ρ_c = molten cladding density.

The CLAP model has a hysteresis effect in the treatment of the flooding multiplier whereby flooding and the inverse, deflooding, occur at slightly different velocities as follows:

$$\text{set } M^n = M_{2\Phi}, \text{ if } M^{n-1} = 1 \text{ and } \left| w / A_v \rho_v \right| > 1.1 v_{flood} \tag{13.2-8}$$

$$\text{set } M^n = 1, \text{ if } M^{n-1} = M_{2\Phi} \text{ and } \left| w / A_v \rho_v \right| < 0.9 v_{flood} \tag{13.2-9}$$

where *n* is the current time-step number. If the conditions in either Eq. 13.2-8 or 13.2-9 are not met, then the previous value of *M* is retained.

The two-phase friction multiplier is given by

$$M_{2\Phi} = I \cdot \left[1 + \varepsilon \left(1 - \alpha \right) \right] \qquad \text{for } \alpha > \alpha_{crit} \tag{13.2-10a}$$

$$M_{2\Phi} = I \cdot \left[1 + \varepsilon \left(1 - \alpha_{crit} \right) \right] \qquad \text{for } \alpha \le \alpha_{crit} \tag{13.2-10b}$$

where ε and α_{crit} are input and *I* is an incoherence multiplier. For values of ε = 75 and α_{crit} = 0, Eq. 13.2-10 is equivalent to the Wallis correlation [13-5].

Radial incoherency in cladding melting, which occurs during the early portion of cladding motion, results in a lower bundle pressure drop and lower cladding velocity than predicted by one-dimensional models that ignore this effect [13-6]. The incoherence multiplier allows for this incoherency effect by temporarily reducing the two-phase friction multiplier during early cladding motion in the following manner:

$$I = \left[fps / \left(fps \right)_0 \right]^x \qquad \text{for } fps < \left(fps \right)_0 \tag{13.2-11a}$$

$$I = 1 \qquad \text{for } fps \ge \left(fps \right)_0 \tag{13.2-11b}$$

where *fps* are full-power seconds since cladding first moved in a channel and $(fps)_0$ and *x* are input constants.

The code sets $M_{2\varphi}$ equal to unity, equivalent to a smooth wall friction factor, if the value of $M_{2\varphi}$ computed by Eq. 13.2-10 is less than unity. Consequently, the effect of the multiplier "*I*" is to delay flooding by $(fps)_0$ full-power seconds. For cases where the vapor velocity is below that necessary for flooding, neither $(fps)_0$ nor ε will have any effect on the cladding motion. Values for $(fps)_0$ and *x* of 0.3 and 3 are provisionally recommended; better values will be determined later by calibration of the CLAP model using experimental data.

13.2.2 Moving Cladding Basic Equations

The mass, momentum, and energy conservation equations for moving (molten) cladding are

$$\frac{\partial}{\partial t}\left(\rho_c A_c\right) + \frac{\partial}{\partial z}\left(\rho_c A_c v_c\right) = \dot{m}_c \tag{13.2-12}$$

$$\frac{\partial}{\partial t}\left(\rho_c A_c c_c\right) + \frac{\partial}{\partial z}\left(\rho_c A_c v_c^2\right) + A_c \frac{\partial p}{\partial z}$$

$$+ A_c F_p - A_v F_v + A_c \rho_c g = \begin{cases} \dot{m}_c v_c \text{ if freezing} & \text{(13.2-13a)} \\ 0, \quad \text{if melting} & \text{(13.2-13b)} \end{cases}$$

$$\frac{\partial}{\partial t}\left(\rho_c A_c e_c\right) + \frac{\partial}{\partial z}\left(\rho_c A_c v_c e_c\right) = \phi_c P_r + \dot{m}_c e_c \tag{13.2-14}$$

A_c = moving cladding cross-sectional area

v_c = moving cladding velocity

$\dot{m}_c$ = mass rate of melting of substrate per unit length of channel (or rate of freezing if negative)

F_p = pin friction-force per unit volume of molten cladding

e_c = moving cladding internal energy

ϕ_c = flux of sensible heat from the solid/liquid interface into the molten cladding

P_r = perimeter of solid/liquid interface.

The pin or bare-fuel friction force is evaluated by the following:

$$F_p = c_f \rho_c v_c |v_c| / 2D_c \tag{13.2-15}$$

where

c_f = pin friction factor

D_c = molten cladding hydraulic diameter.

The CLAZAS [13-3] formulation for the friction factor has been incorporated into CLAP:

$$c_f = 64/\mathrm{Re} \qquad \text{for } \mathrm{Re} < (\mathrm{Re})_{break} \tag{13.2-16a}$$

$$c_f = b_f \qquad \text{for } \mathrm{Re} \geq (\mathrm{Re})_{break} \tag{13.2-16b}$$

where Re is the molten-cladding Reynolds number defined by:

$$\mathrm{Re} = \frac{D_c \rho_c |v_c|}{\mu_c} \tag{13.2-17}$$

$(\mathrm{Re})_{break}$ is the critical Reynolds number for the transition from laminar to turbulent friction and b_f is the turbulent Moody friction factor. The CLAZAS derived values for $(\mathrm{Re})_{break}$ and b_f of 2.1 x 10^3 and 2.0 x 10^{-2} are currently recommended as input values.

The cladding viscosity depends upon the cladding temperature T_c and melt-fraction f as follows

$$\mu_c = \mu_m \exp(a/T_c - a/T_m) \qquad \text{for } T_c > T_m \tag{13.2-18a}$$

$$\mu_c = (\mu_t - \mu_m)(1-f)^q + \mu_m \qquad \text{for } T_c = T_m \tag{13.2-18b}$$

$$\mu_c = \mu_s \qquad \text{for } T_c < T_m \tag{13.2-18c}$$

where T_m is the cladding melting temperature, μ_s, μ_t, μ_m are the user-supplied viscosities for solid cladding, at the solidus temperature, and cladding at the liquidus temperature, and a and q are input constants. Values for μ_m and a of 6.42 x 10^{-3} Pa·s and 5492 K are recommended [13-7]. The input parameters μ_t, μ_s, and q are not properties per se, but are constants in a phenomenological model and hence need to be determined by calibration with cladding motion test data. In general, the values selected for μ_t and μ_s should be sufficiently large to effectively arrest cladding motion for solid cladding. Provisional values for both μ_t and μ_s of 10^4 Pa·s (10^5 poise), from the CLAZAS sample problem [13-3], and for q of 0.5 are recommended.

The momentum and energy Eqs. 13.2-13 and 13.2-14 are converted to non-conservative form using Eq. 13.2-12, giving the following:

$$\rho_c \left[\frac{\partial v_c}{\partial t} + v_c \frac{\partial v_c}{\partial t}\right] + \frac{\partial p}{\partial z} + F_p - \frac{A_v}{A_c} F_v + g\rho_c = \begin{cases} 0 & \text{if freezing} \qquad (13.2\text{-}19a) \\ -m_c \dot{v}_c / A_c & \text{if melting} \qquad (13.2\text{-}19b) \end{cases}$$

$$\frac{\partial e_c}{\partial t} + v_c \frac{\partial e_c}{\partial z} = \frac{\phi_c P_r}{A_c \rho_c} \tag{13.2-20}$$

13.2.3 Refrozen Cladding Basic Equations

The conservation equations for the refrozen steel layer are

$$\frac{\partial}{\partial t}\left(\rho_s A_s\right) = -\dot{m}_c \tag{13.2-21}$$

$$\frac{\partial}{\partial t}\left(\rho_s A_s e_s\right) = \phi_r P_e - \phi P_r - \dot{m}_e e_s \tag{13.2-22}$$

where

ρ_s = refrozen steel density

A_s = refrozen steel cross-sectional area

e_s = refrozen steel internal energy

ϕ_r = heat flux at the interface between intact cladding and refrozen cladding

P_e = outer perimeter of intact cladding

ϕ = flux of sensible heat from the refrozen cladding to the melt (solid/liquid) interface.

Recall that the quantity $\dot{m}_c$ was the rate of melting (negative for freezing) and hence appears as a sink (negative sign) in the refrozen cladding Eqs. 13.2-21 and 13.2-22.

By manipulating the preceding equations, we obtain the nonconservative form of the energy equation:

$$\frac{\partial e_s}{\partial t} = \frac{(\phi_r P_e - \phi P_r)}{\rho_s A_s} \tag{13.2-23}$$

Note that the sensible heat fluxes on either side of the melt layer are not the same (see Fig. 13.2-1b). The difference ϕ_{hf} is the heat flux for fusion, defined by

$$\phi_{hf} = \phi - \phi_c \tag{13.2-24}$$

The rate of melting (or freezing, if negative) is directly related to the fusion heat flux:

$$\dot{m}_c = P_r \phi_{hf} / \lambda \tag{13.2-25}$$

where λ is an effective heat of fusion of the cladding defined as

$$\lambda = e_c - e_s \tag{13.2-26}$$

13.2.4 Heat-transfer Relationships

13.2.4.1 Moving Cladding on Bare Fuel

The configuration in the molten zone is shown in Fig. 13.2-1a. There is no solid cladding in this region and, therefore, the heat flux for melting, ϕ_{hf}, is zero. The sensible heat flux is given by

$$\phi_c = h\left(T_f - T_c\right) \tag{13.2-27}$$

where

T_f = fuel pellet surface temperature

h = coefficient of heat transfer from the fuel to molten cladding.

The heat-transfer coefficient for the moving cladding is defined from a correlation for liquid-metal heat transport as

$$hD_c / k_c = C_1\left(D_c \rho_c c_{pc} |v_c| / k_c\right)^{C_2} + C_3 \tag{13.2-28}$$

where

k_c = molten cladding thermal conductivity

c_{pc} = molten cladding specific heat capacity

C_1, C_2, C_3 = input constants.

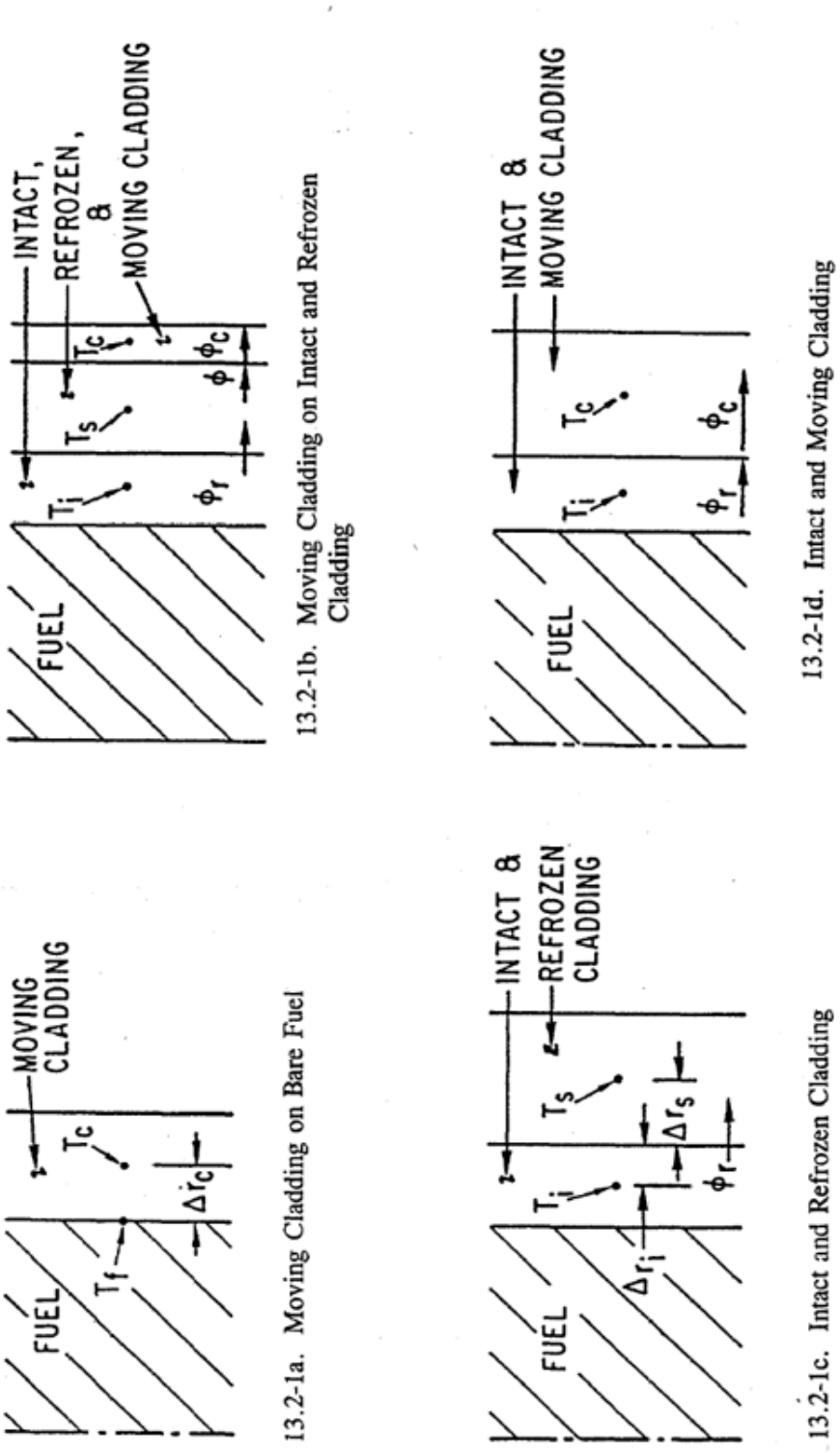

13.2-1a. Moving Cladding on Bare Fuel

13.2-1b. Moving Cladding on Intact and Refrozen Cladding

13.2-1c. Intact and Refrozen Cladding

13.2-1d. Intact and Moving Cladding

Fig. 13.2-1. Schematic Showing the Different Heat-Transfer Configuration in CLAP

The same correlation and constants are used for computing heat-transfer coefficients for single-phase sodium flow in the channel, (Eq. 3.3-9 of Chapter 3). The correlation of Maresca and Dwyer [13-8] for in-line flow in rod bundles is recommended, for which the constants are:

$$C_1 = 0.0155\left(\overline{\psi}\right)^{0.86} \tag{13.2-29a}$$

$$C_1 = 0.86 \tag{13.2-29b}$$

$$C_3 = 6.66 + 3.126\left(P/D\right) + 1.184\left(P/D\right)^2 \tag{13.2-29c}$$

where $\overline{\psi}$ = mean ratio of the thermal and momentum diffusivities, and P/D = rod pitch-to-diameter ratio. Since the code does not allow for flow-rate-dependent values for C_1, it is suggested that $\overline{\psi}$ be set equal to unity in Eq. 13.2-29a with the understanding that the resulting heat-transfer coefficients will be slightly overestimated.

13.2.4.2 Moving Cladding on Intact and Refrozen Cladding

Various configurations can exist in the region outside the molten zone, depending upon whether or not moving cladding and/or refrozen cladding are present in addition to the original intact solid cladding. In this subsection, we consider the case where all three components are present (see Fig. 13.2-1b). The various heat fluxes shown in the figure are given by

$$\phi_r = k_c\left(T_i - T_s\right)/\left(\Delta r_i + \Delta r_s\right) \tag{13.2-30}$$

$$\phi_r = k_c\left(T_s - T_m\right)/\Delta r_s \tag{13.2-31}$$

$$\phi_c = h\left(T_m - T_c\right) \tag{13.2-32}$$

where

T_i = temperature of the intact solid cladding

T_s = temperature of the refrozen cladding

T_m = cladding melting temperature

Δr_i = half-thickness of the intact solid cladding

Δr_s = half-thickness of the refrozen cladding.

The film coefficient formula is identical to Eq. 13.2-28 and the fusion heat flux ϕ_{hf} is given by Eq. 13.2-24.

13.2.4.3 Intact and Refrozen Cladding

In the absence of moving cladding (see Fig. 13.2-1c), we set ϕ = 0 and ϕ_{hf} = 0. The heat transfer between the initial and refrozen cladding is computed from

$$\phi_r = k_c \left(T_i - T_s\right)/\left(\Delta r_i + \Delta r_s\right) \tag{13.2-33}$$

which is identical to Eq. 13.2-30.

13.2.4.4 Intact and Moving Cladding

The moving cladding may be sufficiently hot to melt through the layer of refrozen cladding; this results in the configuration (see Fig. 13.2-1d) in which just the intact cladding and moving cladding are present. In the numerical model this situation also arises when moving cladding first contacts the intact cladding in an axial segment, in which case refrozen cladding is formed and will be present in the next time step.

The heat fluxes ϕ_1 and ϕ_2 and trial heat flux are calculated as follows

$$\phi_1 = k_c \left(T_i - T_m\right)\Delta r_i \tag{13.2-34}$$

$$\phi_2 = h\left(T_m - T_c\right) \tag{13.2-35}$$

$$\phi_{trial} = \phi_1 - \phi_2 \tag{13.2-36}$$

Recalling that ϕ_r is the outer surface heat flux for the initial cladding, ϕ_c the sensible heat flux for moving cladding, and ϕ_{hf} the latent heat flux associated with refrozen cladding, we have

$$\phi_{hf} = 0, \phi_r = \phi_2, \text{ and } \phi_c = \phi_2 \qquad \text{for } \phi_{trial} \geq 0 \tag{13.2-37a}$$

$$\phi_{hf} = \phi_{trial}, \phi_r = \phi_1, \text{and } \phi_c = \phi_2 \qquad \text{for } \phi_{trial} < 0 \tag{13.2-37b}$$

13.2.5 Cladding Physical Properties Relationships

The density of the solid and liquid cladding are assumed to be linear functions of temperature:

$$\rho_s = \rho_s^0 \left[1 - 3\beta\left(T - T_{ref}\right)\right] \tag{13.2-38}$$

$$\rho_c = \rho_c^0 \left[1 - C\left(T - T_m\right)\right] \tag{13.2-39}$$

where

ρ_s^0 = density of solid cladding at reference temperature T_{ref}

ρ_c^0 = density of cladding at the liquidus temperature

β = linear coefficient of thermal expansion for solid

C = volumetric coefficient of thermal expansion for liquid.

For partly-molten cladding, the density is evaluated using

$$\rho = \left[\left(1 - f\right)/\rho_s\left(T_m\right) + f/\rho_c\right]^{-1} \tag{13.2-40}$$

where f is the melt fraction as defined by Eq. 13.2-43.

The internal energies of the solid and molten cladding are also assumed to be linear functions of temperature

$$e_s = c_{ps} T \tag{13.2-41}$$

$$e_c = e_c^o + c_{pc} T \tag{13.2-42}$$

where $e_c^o = \lambda^o + \left(C_{ps} - C_{pc}\right) T_m$, and $\lambda^o =$ heat of fusion. For mixtures, the mass melt fraction is given by

$$f = \left(e - c_{ps} T_m\right)/\lambda^o \tag{13.2-43}$$

13.3 Method of Solution

13.3.1 CLAP Initialization and Cladding Meltthrough

The temperature and melt fraction of initial cladding are computed after the onset of boiling by the SAS fuel-pin model located in the subroutine TSHTRV and the calculation continues after CLAP initiation. This subroutine also contains the logical statements for CLAP initiation and cladding melt-through.

The first cladding to move is assumed to be the first axial segment that is completely molten; CLAP is initiated with this first melt-through. Any other axial segments join the molten cladding region if any one of its three radial segment nodes is molten; i.e., is above the liquidus temperature.

When entering CLAP (which uses coolant time steps) from a heat-transfer time step, a check is made to see whether any previously solid cladding nodes are now to be treated as molten cladding. If so, the total mass and energy of the initial, refrozen, and moving cladding are evaluated and these become the mass and energy of the moving cladding.

13.3.2 Solution of the Cladding Energy Equations

13.3.2.1 Interface with the Fuel-pin Model

There are slight differences in the thermodynamic representations of molten steel in the fuel-pin and CLAP models. In particular, the fuel-pin model in subroutine TSHTRV has a melting band (discrete solidus and liquidus temperatures) and a temperature-dependent specific heat, whereas CLAP has a single melting temperature and constant specific heats. If cladding temperatures from the fuel-pin model were used directly in CLAP calculations (for example, in adding segments to the molten region), then, possibly, energy would not be conserved due to differences in the thermodynamic models. To insure energy conservation, CLAP instead uses nodal energies rather than temperatures. A mean energy is computed from the SAS nodal energies:

$$\bar{e}_j = \frac{1}{4} e_{1,j} + \frac{1}{2} e_{2,j} + \frac{1}{4} e_{3,j} \tag{13.3-1}$$

where the $e_{i,j}$'s are the energies of the three radial nodes in axial segment j. CLAP then evaluates the intact-cladding temperature T_i and melt fraction using $\bar{e}$ and Eqs. 13.2-41 to 13.2-43.

The fuel-pin model computes fuel temperatures in the molten cladding zone and both fuel and intact cladding temperatures for the remainder of the fueled section. For the molten zone, the CLAP routine integrates the fuel surface heat loss for each segment for a heat-transfer time interval:

$$Q_j = P_r \Delta z_j \int_{t^*}^{t^* + \Delta t^*} \phi_{c,j} dt \tag{13.3-2}$$

where

$\Delta z_j = z_{j+1} - z_j$

t^* is time at start of current heat-transfer time step

Δt^* is current heat-transfer time interval

ϕ_c is the heat flux given by Eq. 13.2-27

z_j is the elevation at the bottom of the "j"th segment.

This heat loss is utilized at the outer fuel boundary condition by the fuel-pin model. In a similar fashion, the heat loss from the outer surface of an intact cladding segment is computed by

$$Q_j = P_e \Delta z_j \int_{t^*}^{t^*+\Delta t^*} \phi_{r,j}\, dt \tag{13.3-3}$$

where ϕ_r is the heat flux from Eq. 13.2-30 or 13.2-37, depending upon the configuration. This heat loss becomes part of the outer cladding boundary condition in the fuel-pin model, being added to the coolant heat loss, if any.

13.3.2.2 Intact and Refrozen Cladding

For this configuration, we set ϕ = 0 (adiabatic outer boundary) in the refrozen cladding energy Eq. 13.2-23. The energy equation is then combined with Eqs. 13.2-30 and 13.2-41 to give

$$\frac{dT_{s,j}}{dt} = \xi_1 \left(T_i - T_s\right)\Big|_j \tag{13.3-4}$$

where

$$\xi_{1,j} = P_e k_c \,/\left[A_s \rho_s c_{ps} \left(\Delta r_s + \Delta r_i\right)\right]\Big|_j$$

Since Eq. 13.2-23 has been reduced from a general field equation to a nodal equation, it becomes an ordinary differential equation (in time) in the process. The subscript *j*, of course, denotes the axial segment number for which the parameter is evaluated.

Equation 13.3-4 is converted to an implicit finite difference equation by substituting for the left side, the following:

$$\frac{dT_{s,j}}{dt} \approx \frac{\Delta T_{s,j}^n}{d\Delta} \tag{13.3-5}$$

and by evaluating $T_{s,j}$ on the right side at the advanced time

$$T_{s,j}^{n+1} = T_{s,j}^n + \Delta T_{s,j}^n \tag{13.3-6}$$

giving (after some rearrangement):

$$\Delta T_{s,j}^n = \frac{\xi_1 (T_i - T_s)\Delta t}{1 + \xi_1 \Delta t}\Bigg|_j^n \tag{13.3-7}$$

The implicit form is used rather than an explicit solution because it is stable for large ξ_1 (or small A_s) and a reasonably sized Δt.

The heat flux ϕ_r, required for the fuel-pin boundary condition (Eq. 13.3-3) is evaluated from the energy equation:

$$\phi_{r,j}^{n} = \left.\frac{A_s \rho_s C_{ps} \Delta T_s}{P_e \Delta t}\right|_j^n \tag{13.3-8}$$

13.3.2.3 Evaluation of Convective Term in the Moving Cladding Energy Equation

The CLAP model uses a modified donor cell technique developed by Bohl [13-2] for the evaluation of the convective term

$$C_v = A_c \rho_c v_c \frac{\partial e_c}{\partial z} \tag{13.3-9}$$

in Eq. 13.2-20. This scheme uses a segment boundary mass flow w* which is estimated by

$$w_j^* = \frac{1}{2}\left[A_{c,j-1}\rho_{c,j-1}v_{c,j-1} + A_{c,j}\rho_{c,j}v_{c,j}\right] \tag{13.3-10}$$

The flow direction is determined by a mean flow w_m:

$$w_{m,j} = \frac{1}{2}\left(w_j^* + w_{j+1}^*\right) \tag{13.3-11}$$

The recipe for the convective term for a unblocked segment is as follows

$$C_{v,j} = w_j^* \frac{e_{c,j} - e_{c,j-1}}{z_{m,j} - z_{m,j-1}} \quad \text{for } w_{m,j} > 0, w_j^* > 0 \tag{13.3-12a}$$

$$C_{v,j} = w_{j+1}^* \frac{e_{c,j+1} - e_{c,j}}{z_{m,j+1} - z_{m,j}} \quad \text{for } w_{m,j} < 0, w_{j+1}^* < 0 \tag{13.3-12b}$$

$$C_{v,j} = 0, \text{ otherwise} \tag{13.3-12c}$$

The parameter $z_{m,j}$ is the nodal elevation, which is related to the segment interface elevations z_j by

$$z_{m,j} = \frac{1}{2}\left(z_j + z_{j+1}\right) \tag{13.3-13}$$

If the "*j*"th segment is nearly blocked, then the energy convection computed by Eq. 13.3-12 may be too large in magnitude. In this case, we define a segment flow *w* as

$$w_j = A_{c,j}\,\rho_{c,j}\,v_{c,j} \tag{13.3-14}$$

and compute the convective terms by (blocked segment only)

$$C_{v,j} = w_j \frac{\mathrm{e}_{c,j} - e_{c,j-1}}{z_{m,j} - z_{m,j-1}} \quad \text{for } w_{m,j} > 0, w_j > 0 \tag{13.3-15a}$$

$$C_{v,j} = w_j \frac{\mathrm{e}_{c,j+1} - e_{c,j}}{z_{m,j+1} - z_{m,j}} \quad \text{for } w_{mj} < 0, w_j > 0 \tag{13.3-15b}$$

$$C_{v,j} = 0, \text{ otherwise} \tag{13.3-15c}$$

The scheme also suppresses convection (sets C_v = 0) if the adjoining donor cell (either *j*-1 or *j*+1 depending on the sign of w_m) is blocked.

13.3.2.4 Moving Cladding on Bare Fuel

The outermost radial fuel node in the fuel-pin model is duplicated in CLAP for axial segments within the molten zone. The outer fuel temperature in CLAP, T_f, is reset to the value computed by the pin model at the start of each heat-transfer time step. However, between heat transfer time steps, the fuel temperature is computed in CLAP; this is done primarily to achieve numerical stability, but it may also improve the accuracy of results. The configuration of the SAS outer fuel node and moving cladding is shown in Fig. 13.3-1. The transient heat-balance equation for this outer node is

$$\pi\left(r_{NR}^2 - r_{NT}^2\right)\rho_f c_{pf}\frac{\partial T_f}{\partial t} + 2\pi_{NT}\,k_f\frac{\partial T}{\partial r}\Big|r_{NT} - \pi\left(r_{NR}^2 - r_{NT}^2\right)Q_{NT} = -P_r\,h\left(T_f - T_c\right) \tag{13.3-16}$$

where reference to axial core segment *j* is tacitly implied.

It is assumed that the heat flow from the interior fuel nodes and the heat generated in the outer fuel node (given by the second and third terms in Eq. 13.3016) are relatively constant over one heat-transfer time step. We can therefore approximate these terms by evaluating them at the beginning of a heat-transfer time step. These terms are represented symbolically by the constant C_f, defined by

$$C_f = 2\pi r_{NT}\,k_f\frac{\partial T}{\partial r}\Big|_{r_{NT}} - \pi\left(r_{NR}^2 - r_{NT}^2\right)Q_{NT}, \text{ at } t = t^* \tag{13.3-17}$$

where t^* is the beginning of the heat-transfer time step.

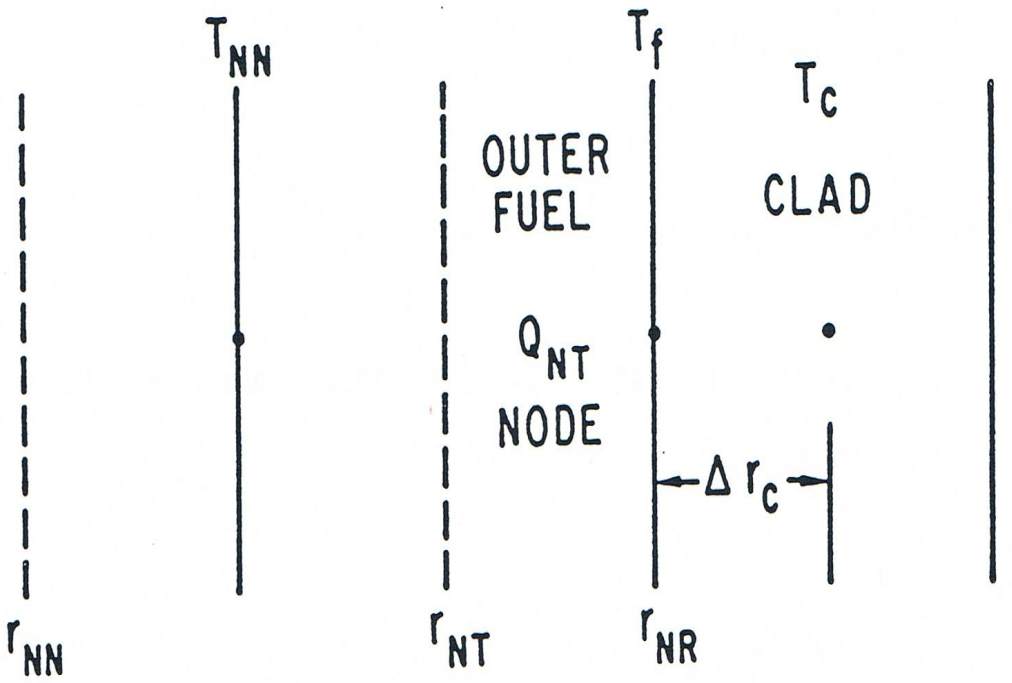

Fig. 13.3-1. Schematic Showing the Interface of CLAP with the SAS Fuel Model

Because of the high heat-transfer coefficient to the molten cladding (Eq. 13.2-28), the fuel-surface temperature and molten cladding temperature are closely coupled. For that reason, the term representing the instantaneous heat loss to the molten steel (on the right side of Eq. 13.3-16) is retained as is, rather than incorporating it into the constant C_f. Combining Eqs. 13.3-16 and 13.3-17 and rearranging, we have

$$\frac{dT_{f,j}}{dt} + \gamma_f = -\xi_f \left(T_f - T_c\right)\Big|_j \tag{13.3-18}$$

where

$$\gamma_{f,j} = C_f / \left[\pi\left(r_{NR}^2 - r_{NT}^2\right)\right]\rho_f c_{pf}\Big|_j \tag{13.3-19}$$

$$\xi_{f,j} = P_r h / \left[\pi\left(r_{NR}^2 - r_{NT}^2\right)\rho_f c_{pf}\right]\Big|_j . \tag{13.3-20}$$

Combining Eqs. 13.2-20, 13.2-27, 13.2-42, and 13.3-9, one obtains the nodal energy equation for moving cladding:

$$\frac{dT_{c,j}}{dt} + \gamma_{c,j} = \xi_2 \left(T_f - T_c\right)\Big|_j \tag{13.3-21}$$

where

$$\gamma_{c,j} = C_v / \left(A_c \rho_c c_{pc}\right)\Big|_j \tag{13.3-22}$$

$$\xi_{2,j} = P_r h / \left(A_c \rho_c c_{pc}\right)\Big|_j \tag{13.3-23}$$

Equations 13.3-18 and 13.3-21 are converted to time-implicit difference equations by approximating the time derivatives according to

$$\frac{dT_{f,j}}{dt} \simeq \frac{\Delta T^n_{f,j}}{\Delta t^n} \tag{13.3-24}$$

$$\frac{dT_{c,j}}{dt} \simeq \frac{\Delta T^n_{c,j}}{\Delta t^n} \tag{13.3-25}$$

and evaluating the temperatures on the right-hand side at the advanced time t^{n+1}. After substituting

$$T^{n+1}_{c,j} = T^n_{f,j} + \Delta T^n_{f,j} \tag{13.3-26}$$

$$T^{n+1}_{c,j} = T^n_{c,j} + \Delta T^n_{c,j}\,, \tag{13.3-27}$$

the two difference equations are solved simultaneously for ΔT_f and ΔT_c and second-order terms in Δt are discarded, with the following results

$$\Delta T^n_{c,j} = -\frac{\left[\xi_2\left(T_f - T_c\right) - \gamma_c\right]\Delta t}{1 + (\xi_2 + \xi_f)\Delta t}\Bigg|^n_j \tag{13.3-28}$$

$$\Delta T^n_{f,j} = -\frac{\left[\xi_f\left(T_f - T_c\right) - \gamma_f\right]\Delta t}{1 + (\xi_2 + \xi_f)\Delta t}\Bigg|^n_j \tag{13.3-29}$$

The heat flux ϕ_c, which is needed to evaluate the integral in Eq. 13.3-2, is computed using a finite difference form of the moving clad energy Eq. 13.2-20:

$$\phi_c = \frac{C_v}{P_r} + \frac{A_c \rho_c c_{pc} \Delta T_c}{P_r \Delta t} \tag{13.3-30}$$

13.3.2.5 Moving Cladding on Intact and Refrozen Cladding

The nodal energy equation for the moving cladding for this configuration is obtained by combining Eqs. 13.2-20, 13.2-32, 13.2-42, and 13.3-9, giving

$$\frac{dT_{c,j}}{dt} + \gamma_c = \xi_2 \left(T_m - T_c\right)\Big|_j \tag{13.3-31}$$

where γ_c and ξ_2 are defined in Eqs. 13.3-22 and 13.3-23.

Solving this equation implicitly, i.e., replacing T_c by the updated value, approximating the time derivative by Eq. 13.3-25, and solving for ΔT_c, we get

$$\Delta T_{c,j}^n = -\frac{[\xi_2 (T_m - T_c) - \gamma_c]\Delta t}{1 + \xi_2 \Delta t}\Bigg|_j^n \tag{13.3-32}$$

The equation for the refrozen cladding temperature is found by substituting Eqs. 13.2-30, 13.2-31, and 13.2-41 into the energy Eq. 13.2-23, resulting in

$$\frac{dT_{s,j}}{dt} = \xi_1 \left(T_1 - T_s\right) - \xi_3 \left(T_s - T_m\right)\Big|_j \tag{13.3-33}$$

where

$$\xi_3 = \frac{P_r k_c}{A_s \rho_s c_{ps} \Delta r_s}. \tag{13.3-34}$$

Converting Eq. 13.3-33 to a finite-difference, implicit equation and solving for ΔT_s, one obtains

$$\Delta T_{s,j}^n = -\frac{[\xi_1 (T_i - T_s) - \xi_3 (T_s - T_m)]\Delta t}{1 + (\xi_1 + \xi_3)\Delta t}\Bigg|_j^n \tag{13.3-35}$$

The heat fluxes ϕ_r and ϕ_{hf} are required for the fuel-pin boundary conditions (Eq. 13.3-3) and to evaluate the rate of melting (Eq. 13.2-25). These are evaluated using discretized versions of the energy Eqs. 13.2-20 and 13.2-23 after computing ϕ_r from Eq. 13.2-30. Then ϕ_{hf} is computed using Eq. 13.2-24.

Several constraints apply to ϕ_{hf}. For positive ϕ_{hf} (melting), more cladding cannot melt than actually exists in a frozen state. This restriction can be expressed as

$$\phi_{hf} \le \frac{A_s \rho_s \lambda_c}{\Delta t P_r} \tag{13.3-36}$$

In case ϕ_{hf} is adjusted to satisfy Eq. 13.3-36, new values of ϕ, ϕ_c and ϕ_r are computed from discretized versions of energy Eqs. 13.2-20 and 13.2-23, along with Eq. 13.2-24, the definition of ϕ_{hf}.

The constraint for negative ϕ_{hf} (freezing) arises from the condition that more cladding cannot freeze then exists in the molten state. Expressed mathematically, the limit is

$$\phi_{hf} \ge -\frac{A_c \rho_c \lambda_c}{\Delta t P_r} \tag{13.3-37}$$

13.3.2.6 Intact and Moving Cladding

The molten cladding energy equation for this case is identical to that for the case of moving cladding on intact and refrozen cladding. The molten cladding temperature change is therefore given by Eq. 13.3-32, which is also displayed below

$$\Delta T_{c,j}^{n} = -\frac{[\xi_2 (T_m - T_c) - \gamma_c]\Delta t}{1 + \xi_2 \Delta t}\Bigg|_j^n \tag{13.3-38}$$

The quantities ϕ_1, ϕ_2, and ϕ_{trial} are computed from Eqs. 13.2-34 to 13.2-36. Then ϕ_{hf} and ϕ_r are computed according to Eq. 13.2-37, which we repeat below

$$\phi_{hf} = 0, \phi_r = \phi_2 \quad \text{for } \phi_{trial} \ge 0, \tag{13.3-39a}$$

$$\phi_{hf} = \phi_{trial}, \phi_r = \phi_1 \quad \text{for } \phi_{trial} < 0. \tag{13.3-39b}$$

The case of $\phi_{trial} \ge 0$ corresponds to melting of the initial cladding; the heat of fusion is included in ϕ_r which is the negative of the heat flux to the pin surface.

For $\phi_{trial} \le 0$, we obtain a negative ϕ_{hf} (freezing) which will result in the appearance of refrozen cladding during the current time step. The constraint given by Eq. 13.3-37 is checked and, if not satisfied, then (i) ϕ_{hf} is set equal to the limit given by Eq. 13.3-37 and (ii) a new ϕ_r is computed by

$$\phi_r = \phi_2 + \phi_{hf} \tag{13.3-40}$$

13.3.2.7 Heat Loss to Structure

At the onset of cladding motion, the structure is still relatively cool and consequently constitutes a potentially significant heat sink for the refreezing of cladding, particularly in small experimental subassemblies. The local heat absorbed by the structure (per unit length and unit time) is given by

$$Q_{s,j}^{n} = \frac{\theta P_w \left(T_m - T_w\right)}{\Delta r_w / k + 1/h} \tag{13.3-41}$$

where

θ = multiplier on heat loss to structure (usually = 1)

P_w = heated perimeter of the structure

T_w = structure temperature

Δr_w = half-thickness of structure.

The present CLAP model allows for the indirect transfer of heat form the moving cladding to the structure by way of the frozen cladding. An adjustment to the refrozen clad temperature ΔT_s is defined by

$$T_{s,j}^{n+1} = \hat{T}_{s,j}^{n+1} + \Delta \hat{T}_{s,j}^{n} \tag{13.3-42}$$

where $\hat{T}_{s,j}^{n+1}$ is the unadjusted refrozen cladding temperature.

Normally, the temperature adjustment would be given by

$$\Delta \hat{T}_{s,j}^{n} = Q_s \frac{\Delta t}{A_s \rho_s c_{ps}}\bigg|_j^n \tag{13.3-43}$$

However, this formulation would be unstable in the case of vanishing A_s or large Δt. To achieve stability, we slightly alter the physics; in particular, T_m is replaced in Eq. 13.3-41 by $T_{s,j}^{n+1}$. This adjustment in T_s is made only for segments where moving cladding is present; and, for these segments, we would expect the frozen cladding temperature to be close to the melting temperature, and hence the error in this approximation would be small. With this modification the adjustment is given by

$$\Delta \hat{T}_{s,j}^{n} = \frac{\xi_w \Delta t^n \left(\Delta \hat{T}_{s,j}^{n+1} - T_w\right)}{1 + \epsilon_w \Delta t^n} \tag{13.3-44}$$

where

$$\xi_w = \left.\frac{\theta P_w}{A_s \rho_s C_{ps}\left(\frac{\Delta r_w}{k}+\frac{1}{h}\right)}\right|_j^n \tag{13.3-45}$$

13.3.3 Refrozen Steel Area Calculation

The refrozen cladding mass conservation Eq. 13.2-21 with the source term given by Eq. 13.2-25 is rewritten in the form

$$\rho_s \frac{\partial A_s}{\partial t} = -\frac{P_r \phi_{hf}}{\lambda} - A_s \frac{\partial \rho_s}{\partial t}. \tag{13.3-46}$$

The finite difference form of this equation is

$$A_{s,j}^{n+1} = A_{s,j}^n - \frac{\left[\left.\frac{\phi_{hf} P_r}{\lambda}\Delta t\right|_j^n + A_{s,j}^n\left(\rho_{s,j}^{n+1} - \rho_{s,j}^n\right)\right]}{\rho_{s,j}^{n+1}} \tag{13.3-47}$$

After the density $\rho_{s,j}^{n+1}$ is evaluated from $T_{s,j}^{n+1}$ using Eq. 13.2-38, then the area $A_{s,j}^{n+1}$ is computed using Eq. 13.3-47. The thickness of the refrozen steel layer is computed from its area by assuming that the refrozen steel forms an annular ring around the intact cladding.

13.3.4 Moving Cladding Area Calculation

The continuity Eq. 13.2-12 and source term (Eq. 13.2-25) are rewritten as

$$\rho_c \frac{\partial A_c}{\partial t} = -A_c \frac{\partial \rho_c}{\partial t} - C_a + \frac{P_r \phi_{hf}}{\lambda} \tag{13.3-48}$$

where

$$C_a = \frac{\partial}{\partial z}\left(\rho_c A_c v_c\right) \tag{13.3-49}$$

The finite difference form of this equation is given by

$$A_{c,j}^{n+1} = A_{c,j}^n + \frac{\left[\left.-A_{c,j}^n\left(\rho_{c,j}^{n+1} - \rho_{c,j}^n\right) - C_a \Delta t_n + \frac{P_r \phi_{hf} \Delta t}{\lambda}\right|_j^n\right]}{\rho_{c,j}^{n+1}} + A_{mod,j}^n \tag{13.3-50}$$

where A_{mod} is a correction term, defined later.

The solution method uses donor-cell differencing to evaluate the convective term C_a in terms of the nodal fluxes w_j (see Eq. 13.3-14) and nodal elevation (see Eq. 13.3-13). Normally $A_{mod} = 0$ and C_a is computed as follows

$$C_a = \frac{\mathrm{w}_{\mathrm{j}}^{\mathrm{n}} - w_{j-1}^{n}}{z_{m,j} - z_{m,j-1}} \quad \text{for } w_{m,j} \geq 0 \tag{13.3-51a}$$

$$C_a = \frac{\mathrm{w}_{\mathrm{j+1}}^{\mathrm{n}} - w_{j}^{n}}{z_{m,j+1} - z_{m,j}} \quad \text{for } w_{m,j} < 0 \tag{13.3-51b}$$

Modifications to this formulation are made (i) to prevent cladding transfer outside of the fuel and blanket region and (ii) to inhibit cladding transfer to flooded or blocked nodes; the modifications consist simply of setting the appropriate values of w_j equal to zero.

Additionally, adjustments must be made for the case where the molten cladding area exceeds the available area A_{max}, defined by

$$A_{\max,j}^{n+1} = A_{f,j} - A_{i,j}^{n+1} - A_{s,j}^{n+1} \tag{13.3-52}$$

where

A_f = total area for cladding allowed by the fuel

A_i = area of the intact cladding (if any).

For the case where the computed $A_{c,j}^{n+1}$ exceeds A_{max}, the following steps are taken: (i) the condition is flagged by setting $NFULL_j$ =1 (initial value is 0), (ii) the molten cladding area $A_{c,j}^{n+1}$ is set equal to $A_{\max}$, and (iii) the computed area for the donor segment is later adjusted consistent with step (ii).

To accomplish step (iii), we first estimate the volume of cladding convected into segment j, denoted by Γ_j, from continuity considerations:

$$\Gamma_j \cong \left[A_{max,j}^{n+1} - A_{c,j}^{n} - \frac{P_r \left. \frac{\phi_{hf} \Delta t}{\lambda} \right|_j^n}{\rho_{c,j}^{n+1}} \right] \bullet \left(z_{j+1} - z_j \right) \tag{13.3-53}$$

Rather than adjusting C_a for the donor cell, we instead set w_j (or w_{j+1}) equal to zero and compute a correction A_{mod}, which is the area change (negative) due to the volume of fluid Γ_j transferred to the flooded cell. For example, for the case of the donor cell below the flooded cell we have

$$w_j = 0,\ A^n_{\text{mod},j-1} = -\Gamma_j / \left(z_j - z_{j-1}\right) \text{ for } NFULL_j = 1,\ w_{m,j-1} \geq 0. \tag{13.3-54}$$

Similarly, for the case of the donor cell above the flooded cell we have

$$w_{j+1} = 0,\ A^n_{\text{mod},j+1} = -\Gamma_j / \left(z_{j+2} - z_{j+1}\right),\ \text{for } NFULL_j = 1,\ w_{m,j+1} < 0. \tag{13.3-55}$$

13.3.5 Reactivity Calculation

The reactivity change due to cladding relocation is computed by

$$\Delta K = \sum_j \left(m^n_j - m^o_j\right) \cdot W_j \tag{13.3-56}$$

where

m^n_j = mass of cladding in the j th segment

m^o_j = original mass of cladding in the j th segment

W_j = cladding reactivity worth distribution.

In the molten region, the mass is computed by

$$m^n_j = A_c \rho_c \Delta z\big|^n_j \tag{13.3-57}$$

$$\text{where } \Delta z_j = z_{j+1} - z_j \tag{13.3-58}$$

Outside the molten region the mass is evaluated using

$$m^n_j = m^0_j + A_s \rho_s \Delta z\big|^n_j + A_c \rho_c\, \Delta z\big|^n_j. \tag{13.3-59}$$

Due to roundoff and other possible small errors, the total mass of cladding may not be absolutely conserved which, if left uncorrected, would create anomalous reactivity effects. To insure mass conservation, the computed mass distribution is renormalized by the following steps:

$$M^n = \sum_j m^n_j, \tag{13.3-60}$$

$$M^o = \sum_j m^o_j, \tag{13.3-61}$$

$$m_j^n \cdot M^o / M^n \rightarrow m_j^n \tag{13.3-62}$$

where the operation A → B indicates that A is substituted for B.

13.3.6 Moving Cladding Velocity Calculation

The cladding momentum equation is solved in a separate subroutine (TSCLD2) that is called after the coolant dynamics equations have been solved. The terms $\partial p/\partial z$ and F_v in the cladding momentum equation are evaluated at time t^n + 1/2 Δt^n (by averaging values at t^n and t^{n+1}) to achieve maximum accuracy with respect to sodium-vapor-induced cladding accelerations.

The pin friction term, $(\partial p/\partial z)_{fr}$, is evaluated at the end of the time step to obtain maximum stability under conditions of strongly accelerating thin cladding films. Substituting

$$v_{c,j}^{n+1} = v_{c,j}^n + \Delta v_{c,j}^n \tag{13.3-63}$$

into Eqs. 13.2-15 and 13.2-16 and retaining only linear terms, we obtain an equation of the form

$$F_{p,j}^{n+1} = y_{1,j}^n + y_{2,j}^n \, \Delta v_{c,j}^n \tag{13.3-64}$$

where

$$y_{1,j}^{n+1} = \frac{32\,\mu_c v_c}{D_c^2}\bigg|_j^n \qquad \text{for } \mathrm{Re}_j^n < (\mathrm{Re})_{break} \tag{13.3-65}$$

$$y_{2,j}^n = \frac{32\,\mu_c}{D_c^2}\bigg|_j^n \qquad \text{for } \mathrm{Re}_j^n < (\mathrm{Re})_{break} \tag{13.3-66}$$

$$y_{1,j}^n = \frac{b_f \rho_c v_c |v_c|}{2D_c}\bigg|_j^n \qquad \text{for } \mathrm{Re}_j^n \geq (\mathrm{Re})_{break} \tag{13.3-67}$$

$$y_{2,j}^n = \frac{b_f \rho_c |v_c|}{D_c}\bigg|_j^n \qquad \text{for } \mathrm{Re}_j^n \geq (\mathrm{Re})_{break} \tag{13.3-68}$$

The parameter C_m is used to represent the momentum convective term

$$C_{m,j} = v_c \frac{\partial v_c}{\partial z}\Big|_j \tag{13.3-69}$$

This parameter is evaluated by alternative formulae depending upon whether the segment is filled with cladding. For *NFULL*(*j*)=1, indicating a filled segment, the term is estimated by the formula

$$C^n_{m,j} = v^n_{c,j} \frac{\partial v_c}{\partial z}\Big|^{n+1/2}_j \tag{13.3-70}$$

where the derivative $\frac{\partial v_c}{\partial z}$ is obtained by rearranging the continuity equation:

$$\frac{\partial v_c}{\partial z} = \frac{1}{\rho_c A_c}\left[\frac{\phi_{hf} P_r}{\lambda} - \frac{\partial(\rho_c A_c)}{\partial t} - v_c \frac{(\rho_c A_c)}{\partial z}\right] \tag{13.3-71}$$

and evaluating at time $t^n + 1/2\,\Delta t^n$. Two alternative equations are obtained, one for each flow direction, as given by the following:

$$\begin{aligned}\frac{\partial v_c}{\partial z_j}\Big|^{n+1/2} = {} & \frac{1}{(\rho_{c,j} A_{c,j})^{n+1/2}}\left[\frac{\phi_{h_f} P_r}{\lambda_c}\Big|^n_j - \rho^n_{c,j}\frac{A^{n+1}_{c,j} - A^n_{c,j}}{\Delta t^n}\right. \\ & \left. - A^n_{c,j}\frac{\rho^{n+1}_{c,j} - \rho^n_{c,j}}{\Delta t^n} - v^n_{c,j}\frac{(\rho_{c,j+1} A_{c,j+1})^{n+1/2} - (\rho_{c,j} A_{c,j})^{n+1/2}}{z_{j+1} - z_j}\right] \\ & \text{for } w^n_{m,j} < 0\end{aligned} \tag{13.3-72}$$

$$\begin{aligned}\frac{\partial v_c}{\partial z_j}\Big|^{n+1/2} = {} & \frac{1}{(\rho_{c,j} A_{c,j})^{n+1/2}}\left[\frac{\phi_{h_f} P_r}{\lambda_c}\Big|^n_j - \rho^n_{c,j}\frac{A^{n+1}_{c,j} - A^n_{c,j}}{\Delta t^n}\right. \\ & \left. - A^n_{c,j}\frac{\rho^{n+1}_{c,j} - \rho^n_{c,j}}{\Delta t^n} - v^n_{c,j}\frac{(\rho_{c,j} A_{c,j})^{n+1/2} - (\rho_{c,j-1} A_{c,j-1})^{n+1/2}}{z_j - z_{j-1}}\right] \\ & \text{for } w^n_{m,j} \geq 0\end{aligned} \tag{13.3-73}$$

where quantities on the right-hand side of Eqs. 13.3-72 and 13.3-73 with the superscript $n+1/2$ are evaluated at time $t^n + \Delta t^{n/2}$ as follows

$$(\ )^{n+1/2} = 1/2\left[(\ )^n + (\ )^{n+1}\right] \tag{13.3-74}$$

For $NFULL_j$=0, indicating an unblocked segment, we use the identity

$$v_c \frac{\partial v_c}{\partial z} = 1/2 \frac{\partial v_c^2}{\partial z} \tag{13.3-75}$$

and evaluate the momentum convection term as follows

$$C_{m,j} = 1/2 \left[\left(v_{c,j+1}^n \right)^2 - \left(v_{c,j}^n \right)^2 \right] / \left(z_{m,j+1} - z_{m,j} \right) \quad \text{for } w_{m,j}^n < 0 \tag{13.3-76}$$

$$C_{m,j} = 1/2 \left[\left(v_{c,j}^n \right)^2 - \left(v_{c,j-1}^n \right)^2 \right] / \left(z_{m,j} - z_{m,j-1} \right) \quad \text{for } w_{m,j}^n \geq 0 \tag{13.3-77}$$

The discretized version of he moving-cladding momentum (Eq. 13.2-19), using the linear approximation for F_p (Eq. 13.3-64), and the symbolic representation for the momentum convective term (Eq. 13.3-69), is given by

$$\left(\rho_{c,j} \right)^{n+1/2} \left[\frac{\Delta v_{c,j}^n}{\Delta t^n} + C_{m,j} + g \right]$$

$$= -\frac{\partial P}{\partial z}\bigg|_j^{n+\frac{1}{2}} - \frac{A_v}{A_c} F_v \bigg|_j^{n+\frac{1}{2}} - y_{1,j}^n - y_{2,j}^n \Delta v_{c,j}^n$$

$$- \begin{cases} 0 & \text{if freezing} \qquad \text{(13.3-78a)} \\ \dfrac{P_{r,j}^n \, \phi_{hf,j}^n \left(v_{c,j}^n + \Delta v_{c,j}^n \right)}{A_{c,j}^{n+1/2} \, \lambda_{c,j}^n} & \text{if melting} \qquad \text{(13.3-78b)} \end{cases}$$

Solving this equation for Δv_c, one obtains the form used in the CLAP program.

13.4 Input-Output Description

A listing of CLAP-related input variables is given in Table 13.4-1 as an aid in preparing or modifying SAS input decks. Additionally, the input items on this list should be rechecked when problems are encountered in the running of SAS cases with cladding motion. This list contains all input items used directly by the following CLAP subroutines: TSCLD1, TSCLD2, SODFRC and DENSIT and, in addition, input items used to initiate CLAP and to calculate reactivity effects due to cladding motion (in subroutine FEEDBK).

The CLAP output appears with both the main full printout and the boiling printout. A sample output is shown in Figure 13.4-1. The output labels are generally self-explanatory. The Fortran variable and units corresponding to each output item are given in Table 13.4-2.

Table 13.4-1. Listing of CLAP-Related Input Parameters

Symbol	Reference Eq. No.	Reference	Block	Location	Recommended Values
T_{ref}	13.2-38	TR	13	419	1700 K
T_m	---	TESOL*	13	810-812	1700 K [13-7]
λ^o	13.2-43	UEMELT	13	816-818	2.703×10^5 J/kg [13-7]
λ^o	13.2-43	UEMELT	13	816-818	2.703×10^5 J/kg [13-7]
C_{ps}	13.2-41	CE	13	1070-1072	690.1 J/kg K [13-7]
		ICLADV	51	17	-
		ICLADB	51	85	1
		IDCLGO	51	125	0
		IDCLSP	51	126	0
		IDCLDE	51	127	0
W_j	13.3-56	CLADRA	62	160-183	-
ρ_s^o	13.2-38	DENSS	63	35	7.256×10^3 kg/m^{3†} [13-7]
C_1, C_2, C_3	13.2-28	C1, C2, C3	64	3-5	Eq. 13.2-28 [13-8]
AFRV,BFRV	13.2-5	AFRV, BFRV	64	168, 169	0.316, -0.25
ρ_c^o	13.2-39	DENS	65	3	6.98×10^3 kg/m^{3†} [13-7]
β	13.2-38	AE	65	4	2.3×10^{-5}/K† [13-7]
C	13.2-39	RHOCD	65	5	8.3×10^{-5}/K† [13-7]
μ_m	13.2-18a	VISMC	65	6	6.42×10^{-3} Pa·s [13-7]
μ_T	13.2-18b	VISTR	65	7	1×10^4 Pa·s [13-3]
μ_s	13.1-18c	VISSC	65	8	1×10^4 Pa·s [13-3]
q	13.2-18b	XVISC	65	9	0.5
b_f	13.2-16b	CLADFR	65	10	0.02 [13-3]
$(Re)_{break}$	13.2-16	REBRK	65	11	2100. [13-3]
ε	13.2-10	GMULTF	65	12	75.0 [13-5]
α_{crit}	13.2-10	ALPHCR	65	13	0.0 [13-5]
$(fps)_o$	13.2-11	FPSO	65	14	0.3s
x	13.2-11a	EXPFPS	65	15	3.0
θ	13.3-41	CLSTHR	65	17	1.0
a	13.2-18a	AVISC	65	20	5492 K [13-7]
c_{pc}	13.2-42	CPC	65	21	621.7 J/kg K† [13-7]

*Orginally TME, but TME is now set equal to the solidus temperature TESOL.
†Evaluated at the melting temperature of 1700 K.

Table 13.4-2. Summary of CLAP Output Items

Item	Symbol	FORTRAN Variable	Units
CLAP Time Step Count	n	ICOUNT	-
Axial Coolant Mode	j	J	-
Main Axial (Nodal) Elevation	$z_{m,j}$	ZFM	m
Refrozen Cladding Thickness	$2\Delta r_s$	RCLAD1	m
Moving Cladding Thickness	$2\Delta r_c$	TCLAD1	m
Intact Cladding Temperature	T_i	TCLAV	K
Refrozen Cladding Temperature	T_s	TEMFS1	K
Moving Cladding Temperature	T_c	TEMMC1	K
Moving Cladding Velocity	V_c	CVEL1	m/s
Coolant Flow Area	A_v	AREAC1	m^2
Internal Flag (=1 in molten zone, =0 otherwise)		LVEL	-

```
CHANNEL   1  SASSA 0.0      RSCASE10
                            SAMPLE OUTPUT FOR SAS DOCUMENT

CLAP OUTPUT, CHANNEL NUMBER  1 TIME = 16.91526 ICOUNT = 892

 AXIAL    MEAN      REFROZEN    MOVING      * * *  TEMPERATURES  * * *    MOVING     COOLANT      TOTAL
COOLANT   AXIAL      CLAD        CLAD      INTACT   REFROZEN    MOVING      CLAD       FLOW        CLAD      INTERNAL
 NODE    ELEVATION  THICKNESS   THICKNESS   CLAD      CLAD       CLAD     VELOCITY     AREA        MASS       FLAGS
  21    1.220D+00  5.340D-04    0.0        1230.0    1222.9     1644.1      0.0       9.742D-06  6.861D-03     0
  20    1.172D+00  5.246D-04    0.0        1534.4    1547.7     1644.1    2.251D-12   1.126D-05  6.240D-03     0
  19    1.124D+00  9.260D-04    0.0        1267.3    1248.6     1644.2    1.996D-11   2.063D-06  9.640D-03     0
  18    1.090D+00  8.427D-04    0.0        1310.7    1281.6     1644.2      0.0       3.912D-06  3.771D-03     0
  17    1.041D+00    0.0        1.415D-04     0.0       0.0     2121.4   -2.142D-01   2.713D-05  1.147D-03     1
  16    9.652D-01    0.0        1.506D-04     0.0       0.0     2184.2   -2.417D-01   2.698D-05  1.216D-03     1
  15    8.890D-01    0.0        1.391D-04     0.0       0.0     2235.8   -2.257D-01   2.717D-05  1.114D-03     1
  14    8.128D-01    0.0        1.593D-04     0.0       0.0     2246.8   -3.034D-01   2.684D-05  1.279D-03     1
  13    7.366D-01    0.0        1.938D-04     0.0       0.0     2171.2   -3.552D-01   2.626D-05  1.579D-03     1
  12    6.604D-01    0.0        1.766D-04     0.0       0.0     2050.7   -3.153D-01   2.655D-05  1.455D-03     1
  11    5.842D-01    0.0        1.758D-04     0.0       0.0     1925.9   -3.437D-01   2.655D-05  1.465D-03     1
  10    5.080D-01  3.593D-05    2.189D-06  1547.4    1627.4     1644.2   -1.727D-03   2.165D-05  4.338D-03     0
   9    4.318D-01    0.0        0.0        1372.6      0.0       0.0       0.0       2.175D-05  3.945D-03     0
   8    3.556D-01    0.0        0.0        1245.8      0.0       0.0       0.0       2.175D-05  3.945D-03     0
   7    2.794D-01    0.0        0.0        1224.1      0.0       0.0       0.0       2.175D-05  3.945D-03     0
   6    2.032D-01    0.0        0.0        1225.4      0.0       0.0       0.0       2.175D-05  3.945D-03     0
   5    1.549D-01    0.0        0.0        1190.2      0.0       0.0       0.0       2.175D-05  1.052D-03     0
   4    1.206D-01    0.0        0.0        1167.8      0.0       0.0       0.0       2.175D-05  2.498D-03     0
   3    7.239D-02    0.0        0.0         956.6      0.0       0.0       0.0       2.175D-05  2.498D-03     0
   2    2.413D-02    0.0        0.0         658.7      0.0       0.0       0.0       2.175D-05  2.498D-03     0
```

Fig. 13.4-1. Sample CLAP Output

REFERENCES

NOTICE

Several references in this document refer to unpublished information. For a list of available open-literature citations, please contact the authors.